Proceedings of the Combustion Institute 40 (2024) 105386

Contents lists available at ScienceDirect

Proceedings of the Combustion Institute

journal homepage: www.elsevier.com/locate/proci

Tabulation-based sample-partitioning adaptive reduced chemistry and cell agglomeration

A. Cuoci [a,*], A. Nobili [a], A. Parente [b,c], T. Grenga [d], H. Pitsch [e]

[a] CRECK Modeling Lab, Department of Chemistry, Materials, and Chemical Engineering, Politecnico di Milano, Italy
[b] Université Libre de Bruxelles, Ecole Polytechnique de Bruxelles, Aero-Thermo-Mechanics Laboratory, Bruxelles, Belgium
[c] WEL Research Institute, 1300 Wavre, Belgium
[d] Faculty of Engineering and Physical Sciences, University of Southampton, UK
[e] Institute for Combustion Technology, RWTH Aachen University, 52056 Aachen, Germany

ARTICLE INFO

Keywords:
Reduced chemistry
Agglomeration
Flame
Soot
Tabulation

ABSTRACT

In this study, we combine the SPARC (Sample-Partitioning Adaptive Reduced Chemistry) and the Cell Agglomeration (CA) techniques, to accelerate the simulation of laminar and turbulent reactive flows with detailed kinetics. The reduced mechanisms adopted by SPARC are generated on the basis of representative thermo-chemical states corresponding to laminar, steady-state flamelets parameterized by the mixture fraction and a progress variable, in line with the TRAC (Tabulated Reactions for Adaptive Chemistry) method, recently proposed by Surapaneni and Mira (Comb and Flame, 2023). To further speed-up the calculation, CA (consisting in grouping the cells having similar thermo-chemical states) is carried out before identifying the local reduced mechanism by means of SPARC. To demonstrate the effectiveness of the approach, we considered two benchmark cases: (i) a laminar, pulsating laminar coflow diffusion flame fueled by a mixture of C_2H_4 and N_2 burning in air; (ii) a 2D, turbulent, non-premixed flame burning n-C_7H_{16} in air subject to decaying isotropic turbulence. In both cases, a detailed kinetic mechanism accounting for the formation of PAHs and soot particles and aggregates was considered. The results are promising, showing both accuracy and computational efficiency. While this study uses non-premixed flamelets with mixture fraction and progress variable as an illustrative example, the proposed methodology has the potential to be applied to various combustion modes, including premixed and partially premixed scenarios.

1. Introduction

Realistic modeling of chemically reactive systems in Computational Fluid Dynamics (CFD) involves a large number of chemical species participating in hundreds/thousands of elementary chemical reactions. The incorporation of detailed chemical kinetics in multi-dimensional CFD remains computationally expensive due to the large number of species and the wide range of timescales of chemical and fluid dynamic processes, resulting in numerical stiffness [1]. To address this challenge, various techniques have been proposed and implemented:

1. Chemical mechanism reduction methods aim to reduce the size of detailed mechanisms while preserving essential combustion characteristics. Approaches based on the DRG technique and quasi-steady-state approximations have been widely employed [1].
2. Dimension reduction techniques focus on identifying low-dimensional attracting manifolds in the composition space, allowing computations in a reduced space [2–4].
3. Storage/retrieval algorithms tabulate combustion chemistry and provide inexpensive approximate solutions, reducing the computational cost of repetitive kinetic calculations [5].
4. Cell agglomeration methods reduce the cost of chemistry calculations by grouping computational cells with similar compositions into zones [6,7]. Each zone represents a group of cells, reducing the total number of zones compared to the number of cells.

CFD solvers based on the operator-splitting strategy are especially suitable for simulation of reactive flows with detailed chemistry [8]. In operator-splitting most of the computational time is spent to solve the chemical step, which consists in solving N independent, stiff, nonlinear systems of ordinary differential equations (ODEs), where N is the

* Corresponding author.
E-mail address: alberto.cuoci@polimi.it (A. Cuoci).

https://doi.org/10.1016/j.proci.2024.105386
Received 4 December 2023; Accepted 11 June 2024
Available online 5 July 2024

number of computational cells:

$$\frac{d\boldsymbol{\psi}}{dt} = \boldsymbol{S}(\boldsymbol{\psi}) \tag{1}$$

where $\boldsymbol{\psi}$ is the thermo-chemical state vector (temperature and composition) in a single computational cell and $\boldsymbol{S}(\boldsymbol{\psi})$ the corresponding rate of change due to the chemical reactions. The independent nature of the ODE systems makes the application of adaptive chemistry techniques straightforward and highly effective. The core idea behind adaptive chemistry is centered around the observation that within small temperature and composition ranges, numerous species have negligible concentrations, and only a limited number of species is chemically active. Consequently, the kinetic mechanism required to describe the chemical evolution within a specific thermo-chemical space may demand fewer species and reactions than the complete mechanism. At the highest level of adaptivity and reduction, the local thermo-chemical state is evaluated *on-the-fly*, and a reduced kinetic mechanism is specifically generated in each cell (DAC, Dynamic Adaptive Chemistry) [9–11]. However, the computational cost of the reduction operations is substantial, especially for higher levels of reduction and complex mechanisms.

To alleviate the additional cost of DAC, the Sample-Partitioning Adaptive Chemistry (SPARC) approach was recently proposed and applied [12]. In SPARC, the *on-the-fly* mechanism reduction overhead is avoided, by building a library of reduced mechanisms in a pre-processing phase to be used in different regions of the domain during the CFD simulation. The challenge lies in effectively partitioning the composition space into clusters, ensuring that each cluster exhibits sufficient homogeneity on a kinetic basis. Several approaches have been considered, from Self Organizing Maps (SOM) to Principal Component Analysis (PCA) [13].

In the present work, we explore the possibility to use low-dimensional manifolds to identify regions with different chemical activities, in line with the TRAC (Tabulated Reactions for Adaptive Chemistry) method, recently proposed in [14]. We applied the pre-partitioning operations on representative thermo-chemical states corresponding to laminar, steady-state flamelets parameterized by the mixture fraction ξ and a normalized progress variable Y_c^n. The advantage over SOM or PCA is that the data generated in the pre-processing phase are now linked to 2 control variables (ξ and Y_c^n) having a clear physical interpretation and direct connection with chemical kinetics. To further speed-up the calculation, Cell Agglomeration (CA) was combined with SPARC. In CA, at each reaction step, the cells with similar properties (*features*) are grouped together in a single zone (*cluster*) with averaged values. Chemistry calculations are carried out per cluster (instead of cells) and the results are mapped back to the original, single cells. Since the number of clusters is usually much smaller than the total number of cells, CA is expected to result in significant computational saving. Instead of using the temperature and selected key-species, the idea is to adopt ξ and Y_c^n as features in CA.

The paper is organized as follows. First, the SPARC and CA techniques based on tabulated chemistry are presented and described (Section 2). Then, in Section 3, two examples of application are presented, analyzed, and discussed: (i) a pulsating, laminar coflow diffusion flame, fed with C_2H_4 in air; (ii) a C_7H_{16}/air turbulent, non-premixed flame subject to decaying isotropic turbulence. In both cases, a detailed kinetic mechanism including formation of soot particles and aggregates was considered.

It is important to note that, even if the these examples are based on non-premixed flamelets parameterized with mixture fraction and progress variable, the proposed methodology is more general and can be extended to other combustion modes such as premixed and partially premixed configurations.

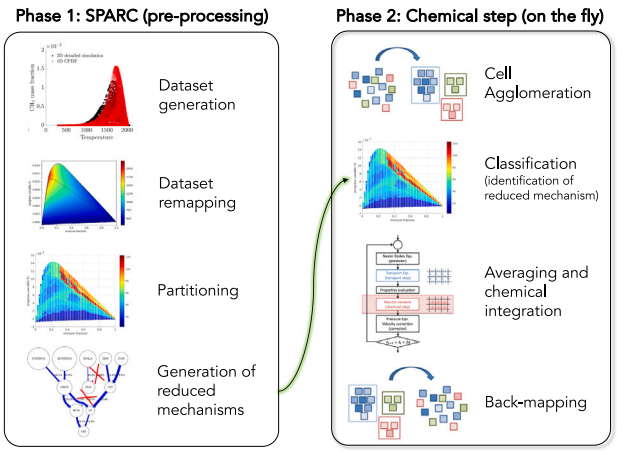

Fig. 1. Tabulation-based sample-partitioning adaptive reduced chemistry and cell agglomeration methodology.

2. Methodology

The proposed procedure consists of 2 phases (Fig. 1). The first phase (SPARC) is carried out as a pre-processing step and aims at generating a library of reduced kinetic mechanisms. The second phase, carried out *on-the-fly*, corresponds to the chemical step in the context of the operator-splitting approach, in which CA is used in combination with the library of kinetic mechanisms produced during the first phase.

2.1. Phase 1: SPARC

The general idea behind SPARC [12] is the assumption that not all the species contained in a detailed kinetic mechanism are (locally) equally necessary. Depending on the physics of the reacting flow, a reduced set of species and reactions can be identified in each cell at each time step.

1. *Dataset generation*: the training dataset must adequately represents all the thermochemical states in the application. Thus, for the cases here presented, it is constructed from steady and unsteady adiabatic diffusion flamelets. The steady flamelets are simulated by varying the applied strain rate until the extinction limit. The composition space between the most strained flamelet and mixing limit is covered by using unsteady flamelets.
2. *Dataset remapping*: the generated database is remapped over two primitive variables to be selected according to the combustion regime and the characteristics of the application. In the examples presented in this paper, we selected the mixture fraction ξ and a normalized progress variable Y_c^n, using a $N_\xi \times N_{Y_c}$ grid with uniform spacing.
3. *Partitioning*: a clustering algorithm in the $\xi - Y_c^n$ space is adopted to identify continuous regions (*i.e.*, clusters) having similar kinetic behavior. In the present work, for simplicity, the $\xi - Y_c^n$ space is decomposed in $N_\xi \times N_{Y_c}$ clusters by means of a regular 2D Cartesian grid. Thus, each cluster is uniquely identified by the ξ and Y_c^n values at its center.
4. *Generation of reduced mechanisms*: for each cluster of the dataset, a reduced mechanism is generated via the DRGEP method [15]. The total number of reduced mechanisms is $N_\xi \times N_{Y_c}$.

Partitioning of the thermochemical space (step 3) can be performed with more advanced approaches, such as Self Organizing Maps (SOM), *k-means* clustering, Local Principal Component Analysis, or PCA-based Artificial Neural Networks (ANN), as demonstrated in [16]. However, since the focus of the paper is on presenting and demonstrating the

applicability of the proposed SPARC-CA methodology, not on assessing the performances of the partitioning algorithm, we adopted the simple 2D Cartesian partitioning mentioned above.

If the partitioning is properly carried out, the individual mechanisms generated for each sample are expected to be very similar. Thus, their union is expected to produce a final mechanism that is not significantly larger than the individual mechanisms. In the ideal case, all the individual simplified mechanisms in a cluster would be identical. Because this almost never happens, a measure of the kinetic similarity must be introduced. If n_{ob} is the number of observations in a given cluster and n_{sp} is the number of species resulting from the union of individual mechanisms, we define $x_i = 1/n_{ob} \sum_{j=1}^{n_{ob}} \delta_{i,j}$, where $\delta_{i,j}$ is equal to 1 if species i is contained in the reduced mechanism for sample j, or equal to 0 if not. Then, for each cluster a *similarity coefficient* is defined as: $\lambda = 1 - 1/n_{sp} \sum_{j=1}^{n_{sp}} (x_i - 1)^2$. λ is equal to 1 in case of perfect uniformity, and its lower bound is 0.

2.2. Phase 2: Chemical step

The second phase is the chemical step of the CFD simulation and includes the following sub-steps:

1. *Cell Agglomeration*: cells having similar thermo-chemical state (identified by ξ and Y_c^n only) are grouped together and the averaged $\bar{\xi}$ and $\bar{Y}_c^n$ are estimated. The Dynamic Multi-Zone (DMZ) algorithm [7], which is based on an unsupervised evolutionary clustering algorithm that automatically determines the optimal number of clusters for a user-defined level of accuracy, is here adopted.
2. *Classification*: based on averaged $\bar{\xi}$ and $\bar{Y}_c^n$, the reduced kinetic mechanism in each cluster is identified from the library built in the pre-processing step.
3. *Averaging and chemical integration*: conservation equations of species and energy are solved according to the reduced kinetic mechanism.
4. *Back-mapping*: the calculated thermo-physical state at the cluster level is mapped back to the original cells, using the backward remapping procedure proposed by Liang et al. [7], which ensures the conservation of mass.

The DMZ algorithm first initializes all the cells as a single, big cluster. Then, the number of clusters evolves since bigger clusters are split in smaller ones via a bisection splitting method. The splitting operations end when the accuracy criteria (*i.e.*, level of thermo-chemical homogeneity of the zones) specified by the user are satisfied. The advantage with respect to static clustering algorithms, such as the k-means algorithm, is that DMZ algorithm does not require *a priori* specification of the final number of clusters. The only input variables required by the DMZ algorithm are a set of *features* (temperature and selected species) and a tolerance ϵ_{CA} (not necessarily the same for all the features) to prescribe the desired level of accuracy.

The averaging process (step 2) consists of calculating the mass-weighted averaged thermo-chemical state $\overline{\boldsymbol{\psi}}^0$ of cells identified as part of a single zone:

$$\overline{\boldsymbol{\psi}}^0 = \frac{\sum_i \boldsymbol{\psi}_i^0 \rho_i V_i}{\sum_i \rho_i V_i} \tag{2}$$

where the sum is carried out over all the cells belonging to the zone and ρ_i and V_i are the density and the volume of cell i, respectively. Then, the reaction step (3), which is the integration of Eq. (1) over the time interval Δt, is carried out for each zone: $\overline{\boldsymbol{\psi}}^0 \longrightarrow \overline{\boldsymbol{\psi}}^*$. Finally, the calculated thermo-physical vector $\overline{\boldsymbol{\psi}}^*$ is mapped back to the original cells. A simple, weighted remapping of the species mass fractions changes from the cluster would gradually deteriorate the solution. For this reason, in the present work we considered a more accurate backward remapping procedure [7], which also ensures conservation of mass. Finally, the cells' temperatures are estimated from the updated mixture sensible enthalpy:

$$H_i^* = H_i^0 + \sum_j h_j^f (\overline{Y}_j^* - \overline{Y}_j^0) \tag{3}$$

where H_i^0 is the mixture sensible enthalpy of cell i before the reaction step, h_j^f is the formation enthalpy of species j and $\overline{Y}_j^0$ and $\overline{Y}_j^*$ the averaged mass fractions before and after the reaction step.

3. Results and discussion

All the simulations have been carried out using the CRECK detailed kinetic mechanism [17], including the chemistry of PAHs (Polycyclic Aromatic Hydrocarbons) and accounting for the formation of soot particles and aggregates via a Discrete Sectional Method (DSM), resulting in a total number of 185 species and about 8000 reactions [18]. The simulations were carried out with the `laminarSMOKE++` code, a CFD solver based on `OpenFOAM`, specifically conceived for reacting flows with detailed kinetic mechanisms [19]. The `laminarSMOKE++` solver is based on the operator splitting technique, making it a suitable candidate for testing the proposed SPARC-CA technique. `laminarSMOKE++` is freely available on the web at the following address: https://github.com/acuoci/laminarSMOKE.

3.1. Generation of training dataset

The training dataset was built from the solutions of steady and unsteady adiabatic laminar flamelets (calculated with the OpenSMOKE++ Suite [20]), from a strain rate of $a = 0.01$ s^{-1} (close to thermodynamic equilibrium), to the extinction, corresponding to $a_q = 250$ s^{-1} (C_2H_4 laminar coflow flame) and $a_q = 120$ s^{-1} (n-C_7H_{16} turbulent diffusion flame). The dataset was parameterized through the mixture fraction ξ and the progress variable $Y_c = \sum_i \alpha_i \frac{Y_i}{W_i}$, where Y_i and W_i are the mass fractions and molecular weights of species CO_2, H_2O, H_2, CO, O_2 and $C_{10}H_8$, with coefficients $\alpha = [1, 1, 0.6, 1, -0.1, 20]$. As demonstrated in [21], the impact of the specific definition of Y_c on the generation of the reduced mechanisms is very limited. Unlike the flamelet methods, in SPARC-CA the chemical source terms and the transport properties are not tabulated, but calculated *on-the-fly* from local conditions using the reduced kinetic mechanisms. Thus, a simple definition of Y_c (such as the linear combination of major products) is expected to be sufficient to identify the evolving thermal states and the reduced kinetic mechanisms.

The chemical reduction was carried out as a pre-processing step using the DRGEP technique [15]. For both the datasets, 7 key-species (fuel, O_2, N_2, OH, BIN5J, BIN13J, and BIN20J) were selected and several tolerance thresholds ϵ_{DRG} were tested. BIN5J, BIN13J, and BIN20J are the sections representing the smallest soot spherical particle, the smallest and the largest soot aggregates, respectively. They were included to properly capture the soot kinetics in the reduction phase. Table 1 reports the average and maximum number of species (respectively n_{sp} and n_{sp}^{max}) as a function of ϵ_{DRG}, together with the mean and the minimum similarity coefficients (λ and λ_{min}, respectively). n_{sp} and n_{sp}^{max} obviously increase with decreasing ϵ_{DRG}. Similarly, the λ coefficient also increases, *i.e.*, the mechanisms in each cluster become more similar.

Fig. 2 presents the maps of mass fractions of soot particles and aggregates stored in the training dataset and the number of species in the reduced kinetic mechanisms as a function of ξ and Y_c for the n-C_7H_{16}/air flame. Similar maps for the C_2H_4 flame are available in the Supplementary Material. The progress variable, ranging from 0 and a maximum $Y_c^{max}(\xi)$, was normalized between 0 and 1:

$$Y_c^n = \frac{Y_c - Y_c^{min}(\xi)}{Y_c^{max}(\xi) - Y_c^{min}(\xi)} \tag{4}$$

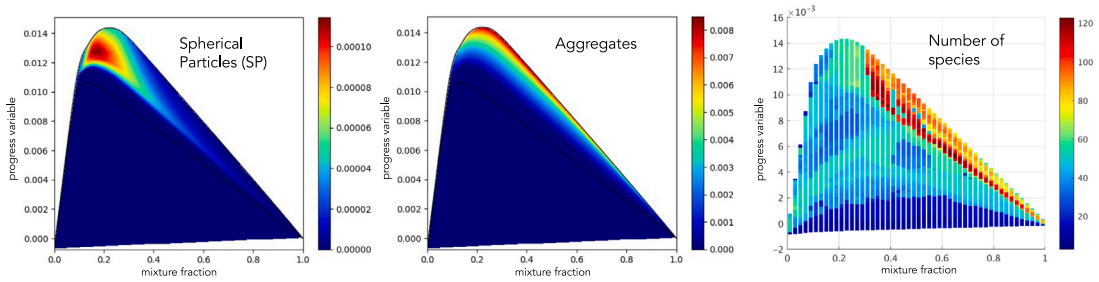

Fig. 2. Mass fractions of soot spherical particles and aggregates and number of species included in the reduced kinetic mechanism as a function of ξ and Y_c for the n-C_7H_{16}/air flame. The dotted line represents the flamelet solution at the extinction scalar dissipation rate a_q.

Table 1
Number of species and similarity coefficients for prescribed tolerances ϵ_{DRGEP} of reduced mechanisms.

	$\epsilon_{DRGEP} = 0.02$				$\epsilon_{DRGEP} = 0.05$				$\epsilon_{DRGEP} = 0.1$			
	n_{sp}	n_{sp}^{max}	λ	λ_{min}	n_{sp}	n_{sp}^{max}	λ	λ_{min}	n_{sp}	n_{sp}^{max}	λ	λ_{min}
C_2H_4	71	136	0.94	0.88	62	110	0.93	0.87	59	98	0.89	0.85
n-C_7H_{16}	70	141	0.94	0.87	59	122	0.92	0.87	53	109	0.89	0.86

The $\xi - Y_c^n$ table was discretized in 40 × 40 cells. The maps show a peak of soot particles at $\xi \sim 0.18$, *i.e.*, at slightly rich conditions (ξ_{st} is 0.143), whereas the soot aggregates cover a very narrow region in the $\xi - Y_c$ space at much larger values of ξ. The highest level of reduction is found in lean regions, *i.e.*, where $\xi < \xi_{st}$, where not more than ~50 active species can be found. Fuel-rich regions, *i.e.*, where $\xi > 0.35$, require more complex chemistry, especially when the scalar dissipation rate is above the extinction value a_q. Moreover, the highest numbers of active species and reactions are found where significant amounts of soot aggregates are predicted. This is strictly related to the intrinsic nature of the DSM adopted for soot: indeed, the chemistry of large aggregates (*i.e.*, BINs larger than BIN13) can be properly described only if smaller BINs are kept in the reduced kinetic mechanism. This prevents the possibility to reach very high levels of chemical reduction, as evident from the data in Table 1.

3.2. Pulsating, laminar C_2H_4 diffusion flame

The first configuration analyzed is an axisymmetric, time-varying, non-premixed laminar coflow flame [22]. The fuel is a mixture of 60% C_2H_4 and 40% N_2 (molar basis), while the oxidizer stream is regular air. Both streams are fed at ambient temperature and atmospheric pressure. The C_2H_4/N_2 fuel stream enters through a circular nozzle (internal diameter of 4 mm and thickness of 0.38 mm), while the coflow air stream enters through an annular region (internal diameter of 50 mm). The transient behavior is induced by a sinusoidal perturbation in the fuel velocity profile with frequency f and amplitude A. Both the fuel and air streams are injected at 35 cm/s. The 2D computational domain (with lengths of 55 mm and 120 mm in the radial and axial directions) was discretized through a Cartesian mesh with ~25,000 cells. The steady-state conditions ($A = 0$) were simulated first, then a sinusoidal fluctuation of the fuel velocity was imposed [22], with $A = 0.90$ and frequencies $f = 10$, 20 and 40 Hz. In the following, only the case with $f = 20$ Hz will be discussed, but the results for the two additional frequencies are available in the Supplementary Material.

Fig. 3 shows the calculated fields of temperature and soot volume fraction and particle number density at different times: maps on the left side refer to the fully-resolved simulation, while maps on the right to simulations carried out with $\epsilon_{DRG} = 0.05$ and $\epsilon_{CA} = 0.04$. The SPARC-CA solution is able to correctly describe on both a qualitative and quantitative basis the complex dynamics of the flame (see for example the pocket of soot leaving the computational domain at t=110 ms).

Different combinations of ϵ_{DRG} and ϵ_{CA} have been investigated, as reported in Table 2, where the relative errors (ϵ) are compared against the fully-resolved simulation. More specifically, the relative error between the SPARC-CA-based (SC) and the fully-resolved (FR) simulations is defined as:

$$\epsilon = \frac{1}{n_T n_C} \sum_{k=1}^{n_T} \sum_{i=1}^{n_C} \frac{\left| \psi_{k,i}^{SC} - \psi_{k,i}^{FR} \right|}{\psi^{max}} \tag{5}$$

where n_T is the number of discrete CFD times, n_C is the number of cells, $\psi_{k,i}$ is the value of ψ (temperature, mass fraction, or soot volume fraction) at time k and cell i and $\psi^{max} = max \left| \psi_{k,i}^{FR} \right|$. Only cells having a temperature $T > 300$ K are included in the sums above, in order to avoid to have a bias in the error estimation. As expected from the theoretical point of view, the results confirm that the relative error decreases monotonically with the tolerances ϵ_{DRG} and ϵ_{CA}. This is an important aspect to control the level of desired accuracy when applying SPARC-CA.

Fig. 4 shows the temporal evolution of the total mass of soot (m_{soot}) and the peak of soot volume fraction (f_V) for the fully-resolved simulation, together with the relative errors when the simulations are performed via SPARC-CA (with $\epsilon_{DRG} = 0.05$) and different values of ϵ_{CA}. Similar plots for cases with f=10 and 40 Hz are available in the Supplementary Material. As expected, the relative error increases for increasing ϵ_{CA}, but it remains consistently small, particularly for m_{soot}. Importantly, it does not exhibit a tendency to accumulate over time. These findings provide a more quantitative affirmation of what could already be inferred from the analysis of Fig. 3, which demonstrates SPARC-CA's capability to accurately describe the soot dynamics, resulting from complex kinetic process.

Additional plots reporting the temperature and mass fraction profiles of selected species at various spatial locations and times, further demonstrating the close agreement between the SPARC-CA and the fully-resolved solutions, are available in the Supplementary Material.

3.3. Turbulent, nonpremixed n-C_7H_{16} flame

The second configuration here adopted is the 2D, turbulent non-premixed flame burning a mixture of n-C_7H_{16} and N_2 (0.844/0.156

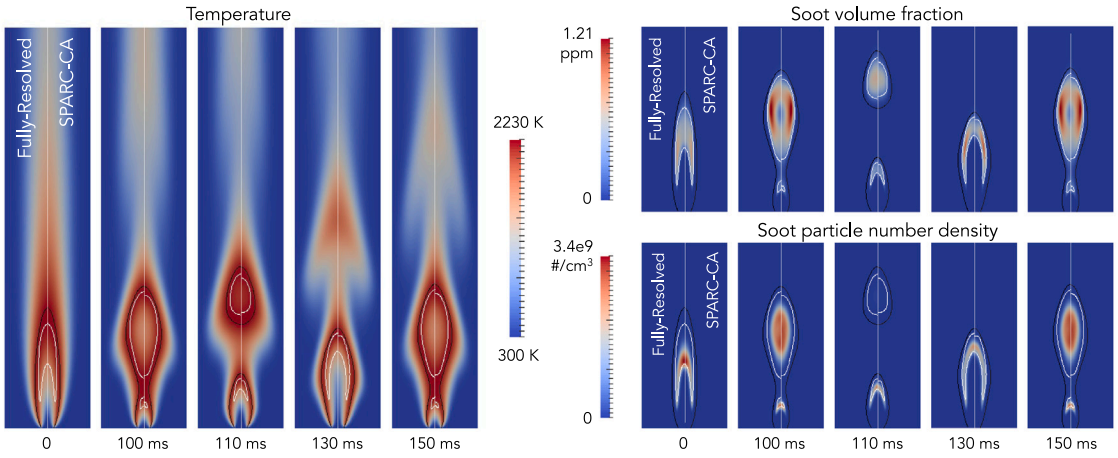

Fig. 3. Pulsating, laminar C_2H_4 diffusion flame: maps of temperature, soot volume fraction f_V and soot particle number density N_s. Fully resolved (FR) and SPARC-CA ($\epsilon_{DRG} = 0.05$ and $\epsilon_{CA} = 0.05$) solutions are reported on the left and right sides, respectively. The black line is the stoichiometric mixture fraction, while the white line the iso-line at $f_V = 0.2$ ppm.

Table 2
Summary of computational performances of SPARC-CA applied to the pulsating laminar coflow flame for several combinations of ϵ_{DRG} and ϵ_{CA} parameters. The relative errors ε are estimated according to Eq. (1). t_{chem} and t_{CA} are the computational times (per time step) for chemical integration and cell-agglomeration, respectively. The time for classification operations is negligible. t_{tot} is the total computational time per time step. SU_c and SU_{tot} are the chemical and the overall speed-up factors, respectively. The computational times are reported in s.

ϵ_{DRG}	ϵ_{CA}	ε_T	ε_{OH}	ε_{CO}	ε_{fv}^{soot}	t_{chem}	t_{CA}	t_{tot}	SU_c	SU_{tot}
(-)	0.01	3.13E−06	3.18E−04	7.78E−05	2.34E−04	3.872	0.002	5.105	5.83	4.7
(-)	0.02	6.28E−06	1.24E−03	1.87E−04	6.29E−04	1.673	0.002	2.916	13.5	8.2
(-)	0.04	8.44E−05	4.55E−03	1.24E−03	1.37E−02	0.742	0.002	1.984	30.3	12.0
0.01	(-)	3.57E−06	6.34E−05	2.73E−05	1.16E−04	8.137	0	9.377	2.78	2.5
0.02	(-)	1.28E−05	4.22E−04	2.08E−04	4.48E−03	4.989	0	6.224	4.53	3.8
0.04	(-)	5.62E−05	2.98E−03	7.07E−04	7.50E−03	2.640	0	3.885	8.57	6.1
0.04	0.01	3.52E−06	3.87E−04	8.72E−05	2.65E−04	2.673	0.002	3.906	8.4	6.1
0.04	0.02	8.23E−06	1.74E−03	2.43E−04	8.67E−04	1.186	0.002	2.429	19.0	9.8
0.04	0.04	1.02E−04	5.15E−03	1.35E−03	1.47E−02	0.542	0.002	1.783	41.5	13.3
0.01	0.04	5.54E−06	8.38E−05	3.49E−05	1.86E−04	1.387	0.006	2.633	16.2	9.1
0.02	0.04	1.67E−05	4.95E−04	2.75E−04	6.07E−03	0.943	0.005	2.183	23.8	10.9

by volume) in air subject to decaying isotropic turbulence, proposed by Bisetti et al. [23]. The 2D computational domain consists of a square of size L=60 mm. Periodic boundary conditions are applied in both the horizontal and vertical directions. At the onset of the simulation, a horizontal strip of fuel is surrounded by the oxidizer. Initial temperature and mass fractions are taken from a representative 1D flamelet solution (at scalar dissipation rate of 60 s^{-1}) and mapped from mixture fraction space onto the vertical coordinate according to the mixture fraction spatial profile. The velocity field is initialized with isotropic turbulence of prescribed fluctuations $u' = 75$ cm/s and integral length $L_{11} = 4.4$ mm. A uniform mesh with 384 × 384 cells was adopted. The solution is advanced up to 15 ms. Because of the high computational cost of this benchmark case, only a limited number of simulations was carried out.

Although referred to as "turbulent", this 2D case does not fully represent three-dimensional turbulence due to its two-dimensional nature. Indeed, this example must be intended as a *proof-of-concept*, aiming at demonstrate the applicability of SPARC-CA to complex fluid dynamic scenarios with very detailed kinetics.

Similarly to Figs. 4, 5 shows the temporal evolution of m_{soot} and f_V. Once again, the same observations made earlier for the C_2H_4 flame can be reiterated. In fact, despite the turbulent nature of the n-C_7H_{16} flame, the relative error on m_{soot} is even lower compared to the C_2H_4. A possible explanation could be related to lower threshold tolerance adopted for the n-C_7H_{16} flame ($\epsilon_{DRG} = 0.01$) with respect to the C_2H_4 flame ($\epsilon_{DRG} = 0.04$), ensuring a generally more accurate reduction of the chemistry. The good agreement between the fully-resolved and the SPARC-CA simulations is also confirmed by the maps of relevant fields (such as soot volume fraction and particle number density) available in the Supplementary Material.

3.4. Analysis of computational time

Table 2 reports details about the computational performance of SPARC-CA applied to the C_2H_4 laminar coflow flame. The overall computational cost (t_{tot}) of SPARC-CA simulations decreases monotonically with increasing tolerances. The time for performing cell-agglomeration operations (t_{CA}) is almost independent of the ϵ_{CA}, but slightly increases with decreasing ϵ_{DRG}, *i.e.* for increasing average number of species in the reduced kinetic mechanisms. However, t_{CA} is a very small fraction of the cost of the chemical step (t_{chem}), which makes cell-agglomeration especially convenient. Being the partitioning carried out on a 2D regular grid in the $\xi - Y_c^n$ space, the additional cost to identify (*i.e.*, to classify) the reduced kinetic mechanism (not reported in the table) is negligible, requiring only the local values of ξ and Y_c^n.

When the complete kinetic mechanism is adopted, ∼95% of total CPU time is spent for performing the chemical step in both the C_2H_4 and n-C_7H_{16} flames. The transport step is not affected by SPARC-CA operations, since all the original species in the complete kinetic mechanism are always transported. Thus, the maximum theoretical

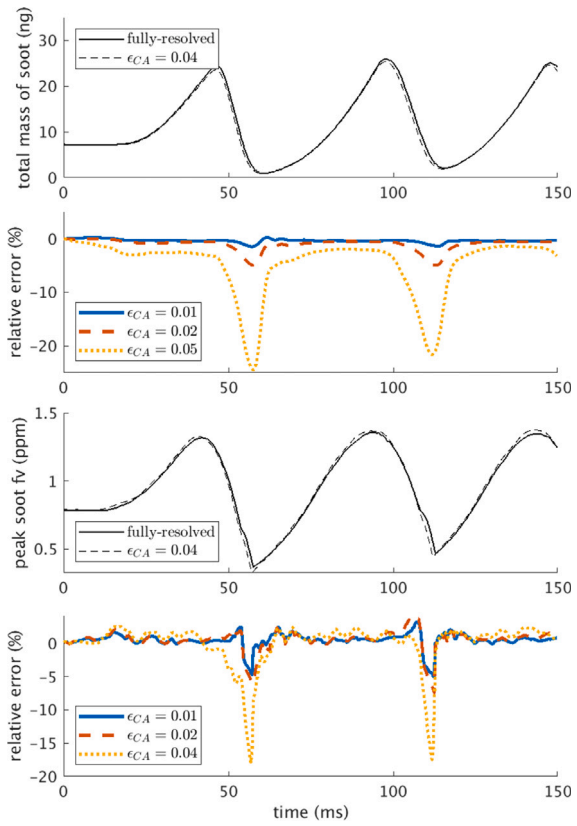

Fig. 4. Pulsating, laminar C_2H_4 diffusion flame: temporal evolution of (a) total mass of soot and (b) peak soot volume fraction for the fully-resolved simulation and relative errors with respect to SPARC-CA simulations.

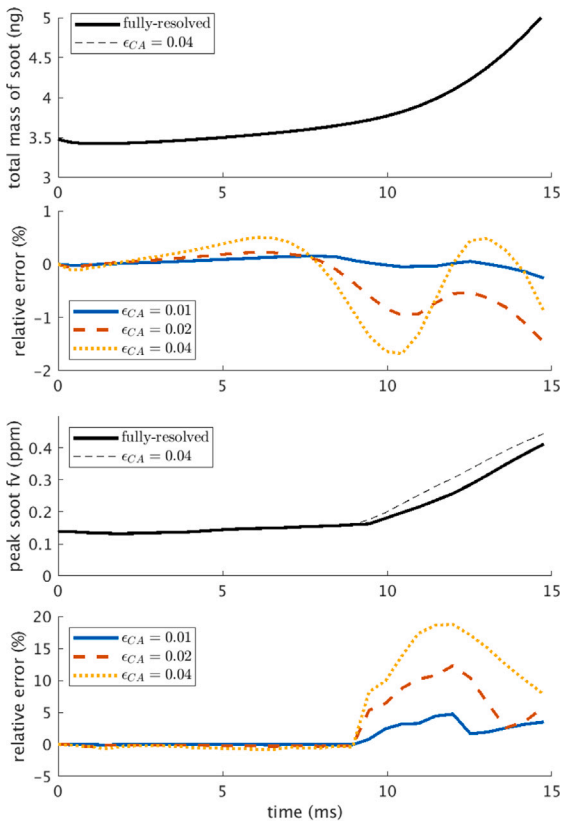

Fig. 5. Turbulent, nonpremixed n-C_7H_{16} flame: temporal evolution of (a) total mass of soot and (b) peak soot volume fraction for the fully-resolved simulation and relative errors with respect to SPARC-CA simulations.

overall speedup which could be reached is ~20. The data reported in Table 2 show that the effective overall speedup increases with increasing tolerances ϵ_{DRG} and ϵ_{CA}, as expected. Indeed, larger tolerances mean smaller average number of species in the reduced mechanisms and smaller number of clusters to be integrated.

The data presented in Table 2 clearly shows that the majority of the overall speed-up, approximately 70%–80%, is attributable to Cell Agglomeration (CA). Consequently, the contribution of Sample Partitioning Adaptive Reduced Chemistry (SPARC) to the overall acceleration (specifically, its role in enabling the use of reduced kinetic mechanisms) is relatively minor compared to CA. However, this finding should not be considered general as it heavily depends on the degree of composition stratification within the specific computational fluid dynamics (CFD) simulation. Notably, CA's effectiveness in accelerating the chemical step increases in scenarios with limited composition stratification, which permits the identification of fewer clusters. Conversely, in simulations with a more varied composition space, the acceleration due to CA is expected to diminish, enhancing the relative impact of SPARC on numerical performance.

Fig. 6 show the temporal evolution of total number of clusters N_c for the C_2H_4 and n-C_7H_{16} flames when different ϵ_{CA} are adopted (with fixed ϵ_{DRG}), together with the corresponding speedup factor S_u. Obviously, N_c decreases with increasing ϵ_{CA}, resulting into an increase of S_u. For the pulsating C_2H_4 flame, both N_c and S_u are almost constant in time, while for the turbulent n-C_7H_{16} flame they are very time-dependent. Indeed, because of the initial stratification in the composition space, at the beginning of the simulation of the n-C_7H_{16} flame cell-agglomeration is very effective, leading to small N_c and large S_u. Then, during the evolution of the system, the composition space covered by the flame becomes larger, which implies an increasing N_c, leading to a reduction of S_u.

4. Conclusions

In this work, we combined the SPARC (Sample-Partitioning Adaptive Reduced Chemistry) and the Cell Agglomeration (CA) techniques with tabulation of chemistry in a 2D space, to accelerate the simulation of laminar and turbulent reactive flows with detailed kinetics. The results, even if preliminary, are satisfactory: the accuracy is good in both the benchmark cases with good levels of acceleration, close to ~70%–80% of theoretical maximum speedup. More systematic and complete analyses are required to better asses the performances and the limitations of the methodology.

While the applications of tabulation-based SPARC-CA presented in this paper were based on non-premixed laminar flamelets (defined by mixture fraction and a progress variable), it is important to emphasize the adaptability of the proposed methodology to broader combustion scenarios, such as premixed and partially premixed modes. The key is using a training dataset that reasonably represents the thermochemical state expected to be found in the CFD simulation and selecting the right variables for effective clustering. A proper training dataset allows to build a solid library of simplified kinetic mechanisms, which makes the simulations more efficient. To better understand the versatility of tabulation-based SPARC-CA, it is also crucial to consider that:

(i) the training dataset is only used to generate a proper library of reduced kinetic mechanisms;
(ii) the remapping based on primitive variables is only used for facilitating a rapid on-the-fly identification of the best reduced kinetic mechanism;
(iii) all the species in the complete kinetic mechanism are transported.

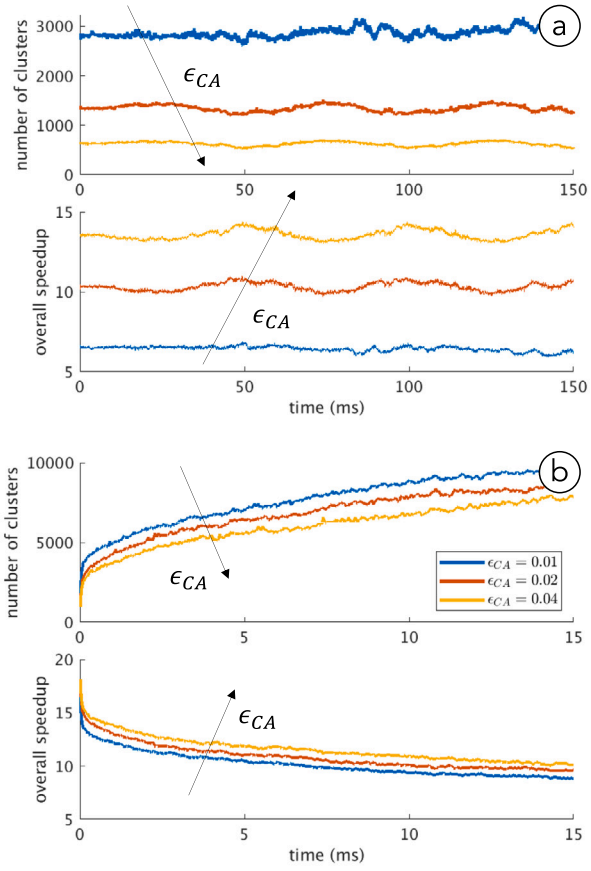

Fig. 6. Time evolution of number of clusters coming from the application of cell-agglomeration (blue line) and of overall speedup factor (red line): (a) pulsating, laminar C2H4 diffusion flame with $\epsilon_{DRG} = 0.05$; (b) turbulent, nonpremixed n-C_7H_{16} flame with $\epsilon_{DRG} = 0.01$. (For interpretation of the references to color in this figure legend, the reader is referred to the web version of this article.)

This means that in the CFD simulations, the thermochemical state is always calculated using detailed (albeit reduced) kinetic mechanisms. Therefore, the training dataset and the identified primitive variables are less crucial compared to tabulated-chemistry approaches, where the thermochemical state is reconstructed from tabulated data.

In conclusion, the tabulation-based SPARC-CA method is a promising technique for accelerating simulations of reactive flows. This methodology ensures good computational efficiency with minimal implementation effort, especially in operator-splitting-based CFD codes. Furthermore, its flexibility allows it to be applied to various combustion regimes, making it a versatile tool for a wide range of applications.

Novelty and significance statement

The main novelty of this research lies in implementation of a new acceleration technique for CFD simulations of reactive flows with detailed kinetic mechanisms. To the authors' knowledge, this is the first time the combination of reduced chemistry and cell agglomeration techniques is implemented and applied on-the-fly in a CFD code. This research is significant because the the proposed acceleration technique has proven capable of ensuring a significant reduction in computation times (speedup factors even larger than 10) while still maintaining good accuracy in both laminar and turbulent simulations. Its adoption could enable simulations with very detailed kinetics that were previously prohibitive or computationally too expensive.

CRediT authorship contribution statement

A. Cuoci: Designed research, Performed the numerical simulations, Writing – original draft, Writing – review & editing. **A. Nobili:** Developed the kinetic mechanism adopted in the simulations, Writing – review & editing. **A. Parente:** Analyzed the numerical results, Writing – review & editing. **T. Grenga:** Analyzed the numerical results, Writing – review & editing. **H. Pitsch:** Analyzed the numerical results, Writing – review & editing.

Declaration of competing interest

The authors declare that they have no known competing financial interests or personal relationships that could have appeared to influence the work reported in this paper.

Acknowledgments

This work was supported by the Alexander von Humboldt Foundation (fellowship for experienced researchers to A. Cuoci). T. Grenga and H. Pitsch acknowledge the support from the European Union's Horizon 2020 research and innovation program under the Center of Excellence in Combustion (CoEC) project, grant agreement no. 952181.

Appendix A. Supplementary data

Supplementary material related to this article can be found online at https://doi.org/10.1016/j.proci.2024.105386.

References

[1] T. Lu, C. Law, Toward accommodating realistic fuel chemistry in large-scale computations, Prog. Energy Combust. Sci. 35 (2) (2009) 192–215.
[2] S. Lam, D. Goussis, The CSP method for simplifying kinetics, Int. J. Chem. Kinet. 26 (4) (1994) 461–486.
[3] W. Sun, Y. Ju, A multi-timescale and correlated dynamic adaptive chemistry and transport (CO-DACT) method for computationally efficient modeling of jet fuel combustion with detailed chemistry and transport, Combust. Flame 184 (2017) 297–311.
[4] T. Grenga, S. Paolucci, M. Valorani, Sensitivity analysis and mechanism simplification using the G-scheme framework, Combust. Flame 189 (2018) 275–287.
[5] S. Pope, Computationally efficient implementation of combustion chemistry using in situ adaptive tabulation, Combust. Theory Model. 1 (1997) 41–63.
[6] G.M. Goldin, Z. Ren, S. Zahirovic, A cell agglomeration algorithm for accelerating detailed chemistry in CFD, Combust. Theory Model. 13 (4) (2009) 721–739.
[7] L. Liang, J. Stevens, J. Farrell, A dynamic adaptive chemistry scheme for reactive flow computations, Proc. Combust. Inst. 32 (2009) 527–534.
[8] Z. Ren, S. Pope, Second-order splitting schemes for a class of reactive systems, J. Comput. Phys. 227 (17) (2008) 8165–8176.
[9] F. Contino, H. Jeanmart, T. Lucchini, G. D'Errico, Coupling of in situ adaptive tabulation and dynamic adaptive chemistry: An effective method for solving combustion in engine simulations, Proc. Combust. Inst. 33 (2) (2011) 3057–3064.
[10] H. Yang, Z. Ren, T. Lu, G. Goldin, Dynamic adaptive chemistry for turbulent flame simulations, Combust. Theory Model. 17 (1) (2013) 167–183.
[11] Z. Ren, C. Xu, T. Lu, M. Singer, Dynamic adaptive chemistry with operator splitting schemes for reactive flow simulations, J. Comput. Phys. 263 (2014) 19–36.
[12] G. D'Alessio, A. Parente, A. Stagni, A. Cuoci, Adaptive chemistry via pre-partitioning of composition space and mechanism reduction, Combust. Flame 211 (2020) 68–82.
[13] I. Jolliffe, Principal component analysis, in: International Encyclopedia of Statistical Science, Springer, 2011, pp. 1094–1096.
[14] A. Surapaneni, D. Mira, Assessment of dynamic adaptive chemistry with tabulated reactions for the simulation of unsteady multiregime combustion phenomena, Combust. Flame 251 (2023) 112715.
[15] P. Pepiot-Desjardins, H. Pitsch, An efficient error-propagation-based reduction method for large chemical kinetic mechanisms, Combust. Flame 154 (1–2) (2008) 67–81.

[16] G. D'Alessio, A. Cuoci, G. Aversano, M. Bracconi, A. Stagni, A. Parente, Impact of the partitioning method on multidimensional adaptive-chemistry simulations, Energies 13 (10) (2020) 2567.
[17] E. Ranzi, A. Frassoldati, A. Stagni, M. Pelucchi, A. Cuoci, T. Faravelli, Reduced kinetic schemes of complex reaction systems: Fossil and biomass-derived transportation fuels, Int. J. Chem. Kinet. 46 (2014) 512–542.
[18] A. Nobili, L.P. Maffei, A. Baggioli, M. Pelucchi, A. Cuoci, C. Cavallotti, T. Faravelli, On the radical behavior of large polycyclic aromatic hydrocarbons in soot formation and oxidation, Combust. Flame 235 (2022) 111692.
[19] A. Cuoci, A. Frassoldati, T. Faravelli, E. Ranzi, Numerical modeling of laminar flames with detailed kinetics based on the operator-splitting method, Energy Fuels 27 (12) (2013) 7730–7753.
[20] A. Cuoci, A. Frassoldati, T. Faravelli, E. Ranzi, OpenSMOKE++: An object-oriented framework for the numerical modeling of reactive systems with detailed kinetic mechanisms, Comput. Phys. Comm. 192 (2015) 237–264.
[21] A. Kalbhor, J. van Oijen, An assessment of the sectional soot model and FGM tabulated chemistry coupling in laminar flame simulations, Combust. Flame 229 (2021) 111381.
[22] R. Mohammed, M. Tanoff, M. Smooke, A. Schaffer, M. Long, Computational and experimental study of a forced, time-varying, axisymmetric, laminar diffusion flame, Symp. (Int.) Combust. 27 (1) (1998) 693–702.
[23] F. Bisetti, G. Blanquart, M.E. Mueller, H. Pitsch, On the formation and early evolution of soot in turbulent nonpremixed flames, Combust. Flame 159 (1) (2012) 317–335.